Spatial heterogeneity of tectonic stress and friction in the crust — **Source link** ↗

Luis Rivera, Hiroo Kanamori

Institutions: California Institute of Technology

Topics: Stress field, Critical resolved shear stress, Earthquake rupture, Focal mechanism and Induced seismicity

Related papers:

- Friction of Rocks

- An improved method for determining the regional stress tensor using earthquake focal mechanism data: Application to the San Fernando Earthquake Sequence

- Use of focal mechanisms to determine stress: A control study

- Crustal stress field in southern California and its implications for fault mechanics

- Determination of stress from slip data: Faults and folds

Spatial heterogeneity of tectonic stress and friction in the crust

Luis Rivera, Hiroo Kanamori

Spatial heterogeneity of tectonic stress and friction in the crust

Luis Rivera[1] and Hiroo Kanamori

Seismological Laboratory, California Institute of Technology, Pasadena, CA, USA

[1] The complex geometry of faults, seismicity, and diversity of earthquake mechanisms suggest that the stress and strength in Earth's crust are spatially heterogeneous. We investigated the degree of heterogeneity using the following two end-member models. In one end-member model, we assumed that the orientation of stress is uniform in the crust as is assumed in many stress inversion studies. In this model, the variability of earthquake mechanisms means that friction during faulting must vary for each event. We computed friction μ from the ratio of the resolved shear stress to the effective normal stress on the fault plane with the assumption of hydrostatic pore pressure. The values of μ vary over a large range from 0 to 1.5. In the other extreme model we assumed optimally oriented slip and a constant $\mu = 0.6$, as is suggested by Byerlee's law, for all the earthquakes, and determined the local stress orientation for each earthquake. The orientation of the stress changes drastically from one earthquake to another, and the assumption of uniform stress field commonly used in stress inversion is not warranted. An important conclusion is that a regionally uniform stress field and constant friction on optimally oriented faults are mutually exclusive. The actual situation in the crust is most likely to be intermediate between these two end-member models. From the existing data alone, we cannot determine the degree of heterogeneity uniquely, but both μ and the local stress field near earthquake faults are likely to vary substantially, and studies on earthquake rupture dynamics must take these heterogeneities into consideration. *INDEX TERMS:* 7209 Seismology: Earthquake dynamics and mechanics; 5104 Physical Properties of Rocks: Fracture and flow; 8010 Structural Geology: Fractures and faults

1. Introduction

[2] The complex geometry of faults, seismicity, and diversity of earthquake mechanisms suggest that the stress and strength in Earth's crust are spatially heterogeneous. However, in stress inversion studies, the orientation of tectonic stress is assumed spatially uniform. Also, the coefficient of friction, μ, is usually considered relatively constant at 0.6. It is thus useful to investigate the degree of spatial heterogeneity of stress and friction. We address this question using the following two end-member models.

[3] In one end-member model, we assume that the orientation of stress is uniform in the crust. This assumption is explicitly used in many stress inversion studies using earthquake data [*Vasseur et al.,* 1983; *Gephart and Forsyth,* 1984; *Lana,* 1986; *Julien and Cornet,* 1986; *Harmsen and Rogers,* 1986; *Carey and Mercier,* 1987; *Michael,* 1987; *Rivera and Cisternas,* 1990; *Horiuchi et al.,* 1995; *Abers and Gephart,* 1997; *Lund and Slunga,* 1999; *Michael,* 2000]. All of them exploit the fact that a single uniform stress field can generate a wide range of focal mechanisms when it is applied

to differently oriented fault planes [*Bott,* 1959; *McKenzie,* 1969; *Celerier,* 1988].

[4] In this method, the basic assumption is that the stress orientation is spatially uniform within the block for which inversion is performed. The inversion yields 4 parameters for the tectonic stress: the orientations of the principal stress axes (3 parameters) and the stress ratio $R = (\sigma_2 - \sigma_3)/(\sigma_1 - \sigma_3)$, where σ_1, σ_2, and σ_3 are the principal stresses.

[5] Since earthquakes occur on fault planes oriented in all directions, the friction, defined by the coefficient of friction μ, must be different on each fault plane, if the orientation of the stress field is uniform. It may appear that if the stress orientation is fixed, we can determine μ uniquely, but as we will show later, μ is also a function of another parameter, $S = \sigma_3/(\sigma_1 - \sigma_3)$.

[6] In the other end-member model we suppose that faulting is optimally oriented and assume a constant μ for all the earthquakes, and determine the local stress orientation for each earthquake. We will show that this model requires a very heterogeneous tectonic stress field.

2. Stress Inversion

[7] To investigate the first end member, we performed inversion of first-motion data originally compiled by the Southern California Seismic Network (SCSN) for the orientation of tectonic stress and the stress ratio, $R = (\sigma_2 - \sigma_3)/(\sigma_1 - \sigma_3)$ with the assumption that the tectonic stress is spatially uniform. We used 1077 events which occurred during the period from 1975 to 1999. These events are shown in Figure 1. To avoid having disproportionately large number of events from a single region, we excluded large events with many aftershocks. Thus, the selection of the events is not entirely objective, but we believe that the spatial coverage shown in Figure 1 is sufficiently uniform to achieve adequate stress inversion. We used the method of *Rivera and Cisternas* [1990] in which the first-motion data, instead of the mechanism solutions, are directly used for inversion. The data are the raw first-motion polarities for a set of events and were provided by SCSN, jointly operated by California Institute of Technology and the U. S. Geological Survey.

[8] The model parameters are the 3 orientation parameters, Φ, Θ, and Ψ for the stress tensor, 1 parameter for the stress ratio R and $2N$ parameters, ϕ_i, and δ_i, $i = 1, 2, \ldots N$, for the fault planes where ϕ_i, and δ_i are the strike and dip of the fault plane of event i, and N is the number of events used for inversion. Then we represent these parameters by a vector

$$\boldsymbol{m} = (\Phi, \Theta, \Psi, R, \phi_i, \delta_i = 1, 2, \ldots N)$$

[9] The method works in two levels; the *bottom level* uses the algorithm described in *Rivera and Cisternas* [1990] where a likelihood function $L(\boldsymbol{m})$ is defined to measure the agreement between the first-motion data and the predicted polarities. In the definition of L, the contribution of each polarity is weighted as a function of the amplitude of the predicted P-wave radiation pattern. The algorithm takes a given starting model $\boldsymbol{m}_o$, uses the gradient of L to sweep the model space, improve the fit, and iterate until a small enough gradient is found. Because of the binary nature of the data and the non-linearity of the problem, the procedure just

[1]Now at EOST-IPGS; Université Louis Pasteur, 5, Rue René Descartes, F67084, Strasbourg, France
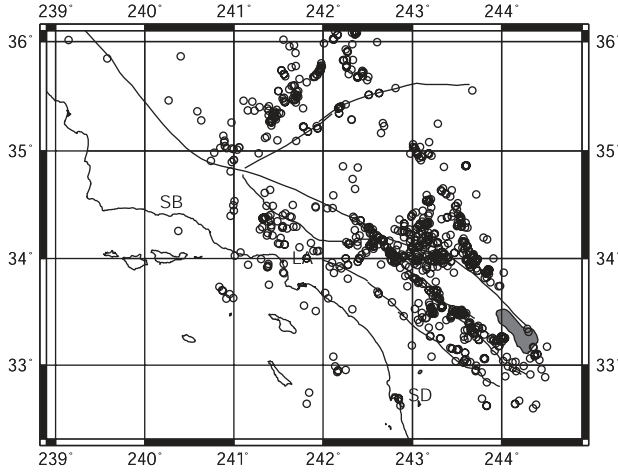
Figure 1. Earthquakes used in this study.

described does not necessarily converge to the best solution, and can settle at a local minimum. Then the *top level* of the method allows us to examine the distribution of local minima. In the *top level*, we generate a set of starting models for the algorithm to work as described above. The stress-related part of the model (Φ, Θ, Ψ, R) is generated randomly and by using a grid-search procedure for each event, we find the fault plane that produces the best fit of the polarity data with the given stress tensor. For each one of these starting models, we run the *bottom level* algorithm and obtain a stationary point of the likelihood function.

[10] From the set of final models obtained by this procedure, we use the corresponding values of L to select the best of them (2%, for example). These best solutions are then plotted on a single figure to show the dispersion of the solutions.

[11] We divided the entire southern California into 5 regions and performed inversion. Figure 2 shows the results for two subregions (the Central Transverse Ranges and the San Jacinto Fault) for which inversion was satisfactory. On each plot the best 20 solutions out of 1000 are shown. For other regions, the inversions were not satisfactory. Since our objective is to investigate the overall distributions of stress and friction, we consider the whole southern California as a single domain. Figure 2 shows the results for the whole southern California. The stress orientations for the whole southern California thus obtained are consistent with the results of other studies [*Abers and Gephart*, 1997; *Brudy et al.*, 1987; *Castillo and Zoback*, 1995; *Hardebeck*, 2001; *Hauksson*, 1990; *Jones*, 1988; *Kerkela and Stock*, 1996; *Zhao et al.*, 1997; *Zoback et al.*, 1987]. A stress ratio $R = 0.5$ is obtained.

3. Friction

[12] The stress orientation and the stress parameter, R, having been determined, we compute the friction on the fault plane of each earthquake. Since the fault planes are oriented in all directions, a significant variation of the friction μ is expected.

[13] Let x_1, x_2, and x_3 be the principal axes, and σ_1, σ_2, and σ_3 the corresponding principal stresses. The stress vector at a point on the fault plane of which the unit normal vector is given by $\vec{n} = (n_1, n_2, n_3)$ is then $\vec{\sigma} = (\sigma_1 n_1, \sigma_2 n_2, \sigma_3 n_3)$. Following the usual convention, compression is taken positive, and $\sigma_1 > \sigma_2 > \sigma_3$ is assumed. Then the magnitudes of the normal stress σ_n and the shear stress σ_t are given by

$$\sigma_n = \sigma_1 n_1^2 + \sigma_2 n_2^2 + \sigma_3 n_3^2 \tag{1}$$

$$\sigma_t = \left(|\vec{\sigma}|^2 - \sigma_n^2 \right)^{1/2} \tag{2}$$

from which, the coefficient of friction is given by

$$\mu = \sigma_t / (\sigma_n - \sigma_p) \tag{3}$$

where σ_p is the pore pressure. In a more general form, $\mu = (\sigma_t - S_o)/(\sigma_n - \sigma_P)$ where S_o is the intrinsic shear strength [e.g. *Jaeger*, 1964, page 76], but for frictional sliding problems at mid-crustal depths where $(\sigma_n - \sigma_P)$ is large, S_o is usually neglected. If S_o is not neglected, μ in (3) must be regarded as the maximum coefficient of friction. Since we do not know the pore pressure σ_P, we write it as $\sigma_P = c(\sigma_1 + \sigma_3)/2$ where c is a constant for each fault. For strike slip events (*i.e.*, $\sigma_2 \sim$ vertical), if the pore pressure is hydrostatic, then $c \approx 1/3$ [e.g. *Jaeger*, 1964, page 121]. Using (1) and (2), (3) can be written as

$$\mu = \frac{\sqrt{K_2 - K^2}}{K + S - c(2S + 1)/2} \tag{4}$$

where $K = n_1^2 + n_2^2 R$, $K_2 = n_1^2 + n_2^2 R^2$, $R = (\sigma_2 - \sigma_3)/(\sigma_1 - \sigma_3)$ and $S = \sigma_3/(\sigma_1 - \sigma_3)$.

[14] From the stress inversion, $\vec{n}$ is determined for each earthquake and R is also determined. Thus, μ can be computed from (4), if S and c are given. This means that μ cannot be determined uniquely from the stress orientation and the stress ratio R; μ is also a function of S, which is not determined by stress inversion. Since the stress inversion can determine only 4 out of the 6 parameters of the stress tensor, two more degrees of freedom (*i.e.*, 2 parameters) are allowed. The parameter S is one of them, and the other is the absolute magnitude of the stress, which is not relevant here. We computed μ for several values of S ranging from 0.4 to 1.5. For a given S, μ is bounded at μ_{max} given by

$$\mu_{max} = \frac{1}{2} \left(S(1 + S) - \frac{c}{2} \left(1 - \frac{c}{2} \right) (1 + 2S)^2 \right)^{-1/2} \tag{5}$$

which is determined from the slope of the tangent, drawn from (σ_p, 0), to a Mohr's circle with a radius of $(\sigma_1 - \sigma_3)/2$ centered at $(\sigma_1 + \sigma_3)/2$.

[15] Figure 3 presents the histograms showing the numbers of events for which friction is given by μ. In this computation, we assumed a hydrostatic pore pressure, *i.e.*, $c = 1/3$. The value of μ_{max} determined from (5) is given on each figure. There is no a priori value for S, except that $S > 0$ (*i.e.*, $\sigma_3 > 0$). The data compiled in the World Stress Map [*Mueller et al.*, 2000] show a large range of S, but the results from the German KTB and the Cajon deep holes
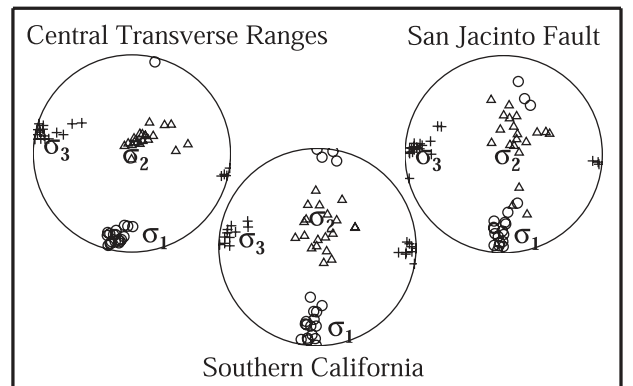

Figure 2. The orientations of the principal axes determined by stress inversion for the Central Transverse Ranges, the San Jacinto Fault, and the entire southern California. The orientations (azimuth, plunge) are as follows. CTR: (σ_1: 191°, 75°, σ_2: 52°, 20°, σ_3: 284°, 78°), SJF: (σ_1: 180°, 69°, σ_2: 36°, 25°, σ_3: 275°, 76°), SC: (σ_1: 185°, 69°, σ_2: 38°, 24°, σ_3: 280°, 78°).

[*Brudy et al.*, 1987; *Zoback and Healy*, 1992] suggest that $S \approx 1$. Figure 3 shows that if $S \approx 1$, then the values of μ vary over a large range from 0 to 0.58.

[16] Laboratory data [*Byerlee*, 1978] and field stress measurements suggest that μ is about 0.6, which is commonly called the Byerlee's law. To test this suggestion, we now assume that μ is constant at 0.6 and compute S for each earthquake. Figure 4 shows the histogram indicating the number of events as a function of S. For many events, S becomes negative. Since σ_3 must be positive at the seismogenic depth, negative values S of are not allowed. Thus, for these events, no solution can be obtained if $\mu = 0.6$. Also, S is bounded at about 1.0 with most of the events between 0.4 and 0.9, which is not consistent with the results from the German KTB and Cajon deep holes.

4. Spatial Heterogeneity of Stress

[17] As the other end member, we now assume that friction μ is constant (at 0.6 for all the events) and that failure occurs on an optimally oriented fault plane, but allow the tectonic stress field to vary spatially.

[18] We first impose the condition that fault is optimally oriented. The stress orientation cannot be determined uniquely unless we know on which nodal plane seismic slip occurred. For most small events, this is not known. However, regardless of the choice of the slip plane, the null-axis of the mechanism solution (*i.e.*, the intersection of the fault plane and the auxiliary plane) is parallel to the intermediate principal stress axis, if the slip occurs in the direction of the shear stress. This can be shown as follows. From (1) and (2), the normal and the shear components of the stress vector on the fault plane can be written as,

$$\vec{\sigma}_n = \sigma_n \begin{pmatrix} n_1 \\ n_2 \\ n_3 \end{pmatrix} = (\sigma_1 - \sigma_3)(K + S) \begin{pmatrix} n_1 \\ n_2 \\ n_3 \end{pmatrix} \quad (6)$$

$$\vec{\sigma}_t = \vec{\sigma} - \vec{\sigma}_n = \begin{pmatrix} \sigma_1 n_1 \\ \sigma_2 n_2 \\ \sigma_3 n_3 \end{pmatrix} - (\sigma_1 - \sigma_3)(K + S) \begin{pmatrix} n_1 \\ n_2 \\ n_3 \end{pmatrix}$$

$$= (\sigma_1 - \sigma_3) \begin{pmatrix} (1 - K)n_1 \\ (R - K)n_2 \\ -Kn_3 \end{pmatrix} \quad (7)$$
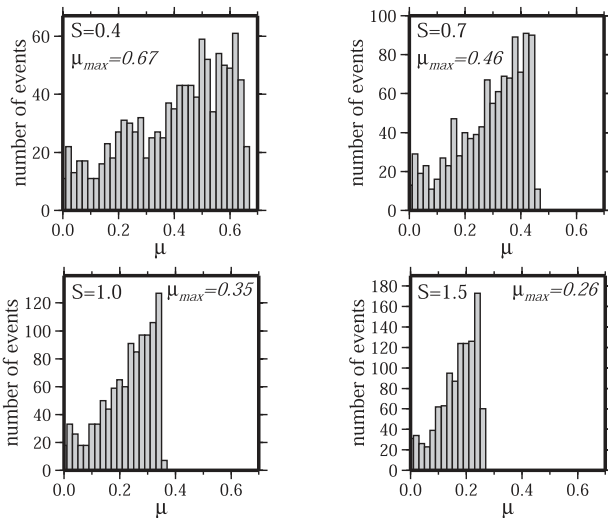
Figure 3. Histograms showing the number of events having friction μ for four values of S. The maximum values of friction allowable for a given S are shown in each figure.
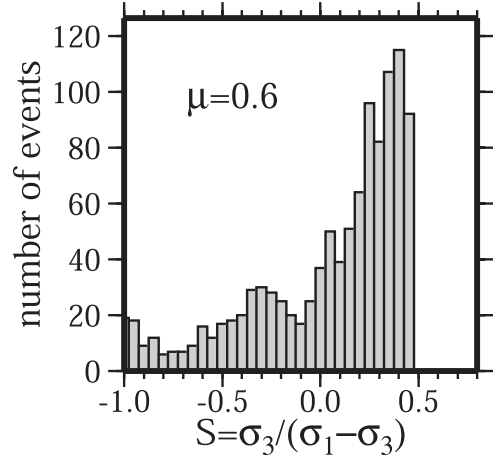
Figure 4. Histograms showing the number of events as a function of S for $\mu = 0.6$. Note that S is negative for many events indicating that no solution exists for these events.

[19] If fracture occurs on the optimally oriented plane, the fault plane contains the intermediate principal stress axis [e.g., *Jaeger*, 1964, page 79], i.e., $n_2 = 0$. Then,

$$\vec{\sigma}_n \propto \begin{pmatrix} n_1 \\ 0 \\ n_3 \end{pmatrix} \text{ and } \vec{\sigma}_t \propto (\sigma_1 - \sigma_3)n_1 \begin{pmatrix} 1 - n_1^2 \\ 0 \\ -n_1 n_3 \end{pmatrix} \propto \begin{pmatrix} n_3 \\ 0 \\ -n_1 \end{pmatrix} \quad (8)$$

[20] Since the null axis of the mechanism is perpendicular both to $\vec{n}$ and $\vec{\sigma}_t$ then (8) implies that it is parallel to the intermediate principal stress axis.

[21] Using this property, we display in the lower-right of Figure 5 the orientation of the intfermediate principal stress axis on a stereographic diagram to show the variability of the stress orientation inferred from earthquake mechanism solutions. For this purpose, we used the mechanism solutions obtained by *Hauksson* [2000]. The stress orientation is extremely heterogeneous, covering almost the entire focal sphere.

[22] Up to this point, we have not yet imposed the condition $\mu = 0.6$. This means that the solutions shown in Figure 5 (lower-right) represent those with any μ including $\mu = 0.6$. Then, if we impose the condition $\mu = 0.6$ we obtain $S = 0.97$ using (5). Thus, the combination of $S = 0.97$ and the intermediate stress axes shown in Figure 5 represents our second end member. The orientation of σ_1 and σ_3 cannot be completely determined because of the nodal planes ambiguity, but plotting both possibilities for the whole set of events produces a wide cloud around a horizontal N-S direction σ_1 for and a horizontal E-W direction for σ_3.

5. Conclusion

[23] The result of this study is summarized in Figure 5, which schematically shows the state of stress and friction in the crust of southern California for the two end-member models we discuss.

[24] An important conclusion is that a regionally uniform stress field and constant friction on every fault are mutually exclusive. If the stress field is uniform, as is commonly assumed in stress inversion studies, the coefficient of friction, μ, must vary over a large range from 0 to 1.5 (the left side of Figure 5). By allowing the ratio $S = \sigma_3/(\sigma_1 - \sigma_3)$ to vary, we could reduce the range of μ and
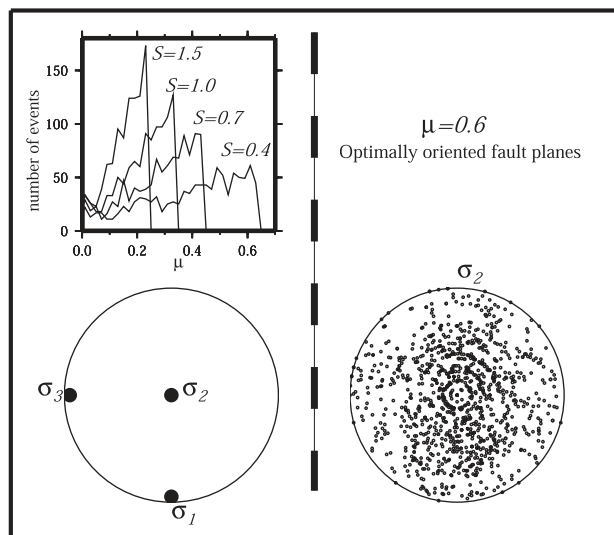
Figure 5. Summary figure showing the two end-member models. The left side shows the model in which a uniform stress is assumed. The lower-left figure shows the orientations of the principal stresses determined by inversion, and the upper-left figure shows the histograms of the events having friction μ for the four models of S. The right side shows the model in which uniform friction μ = 0.6 and optimally oriented fault planes are assumed. The lower-right figure shows the orientations of the intermediate stress axis.

obtain a relatively uniform μ, but in this model the ratio S varies from event to event, which means that the stress field is, after all, heterogeneous.

[25] On the other hand, if we assume that the friction is constant on the fault plane of every earthquake, as is suggested by Byerlee's law, and suppose that failure occurs on optimally oriented planes, then the orientation of the stress must change drastically from one earthquake to another (right side of Figure 5), and the assumption of uniform stress field commonly used in stress inversion is not warranted.

[26] The actual situation in the crust is most likely to be intermediate between these two end-member models. In view of the extreme heterogeneity of friction and stress depicted in these end-member models, it is unlikely that either the stress field or friction is very uniform. From the existing data alone, we cannot determine the degree of heterogeneity, but Figures 3 and 5 suggest that both friction and the local stress field near earthquake faults are likely to vary substantially; the magnitude of stress may also change substantially as suggested by the variation of. Thus, the heterogeneity of stress field and friction in the crust seems to be the essential feature of the crust, and studies on earthquake rupture dynamics must take these heterogeneities into consideration.

References

Abers, G. A., and J. W. Gephart, Stress variations in southern California determined by direct inversion of seismic first motions (MOTSI), *Eos Trans. AGU*, *78*, F451, 1997.

Byerlee, J., Friction of rock, *Pure and Applied Geophysics*, *116*, 615–626, 1978.

Bott, M. P. H., The mechanics of oblique slip faulting, *Geol. Mag.*, *96*, 109–117, 1959.

Brudy, M., M. D. Zoback, K. Fucks, F. Rummel, and J. Baumgartner,

Estimation of the complete stress tensor to 8 km depth in the KTB scientific drill holes: Implications for crustal strength, *J. Geophys. Res.*, *102*, 18,453–18,475, 1987.

Carey, E., and J. L. Mercier, A numerical method for determining the state of stress using focal mechanisms of earthquake populations. Application to Tibetean teleseisms and microseismicity of Southern Perou, *Earth Planet. Sci. Lett.*, *82*, 165–179, 1987.

Castillo, D. A., and M. D. Zoback, Systematic stress variations in the southern San Joaquin Valley and along the White Wolf fault: Implications for the rupture mechanics of the 1952 Ms 7.8 Kern County earthquake and contemporary seismicity, *J. Geophys. Res.*, *100*, 6249–6264, 1995.

Celerier, B., How much does slip on a reactivated fault plane constrain the stress tensor?, *Tectonics*, *7*, 1257–1278, 1988.

Gephart, J. W., and D. W. Forsyth, An improved method for determining the regional stress tensor using earthquake focal mechanism data: Application to the San Fernando earthquake sequence, *J. Geophys. Res.*, *89*, 9305–9320, 1984.

Harmsen, S. C., and A. M. Rogers, Inferences about the local stress field from focal mechanisms: Applications to earthquakes in the southern Great Basin of Nevada, *Bull. Seism. Soc. Am.*, *76*, 1560–1572, 1986.

Hardebeck, J. L., The Crustal Stress Field in Southern California and its Implications for Fault Mechanics, *Ph.D. Thesis*, Seismological Laboratory, Caltech, 2001.

Hauksson, E., Earthquakes, Faulting and Stress in the Los Angeles Basin, *J. Geophys. Res.*, *95*, 15,365–15,394, 1990.

Hauksson, E., Crustal structure and seismicity distribution adjacent to the Pacific and north America plate boundary in southern California, *J. Geophys. Res.*, *105*, 13,875–13,903, 2000.

Horiuchi, S., G. Rocco, and A. Hasegawa, Discrimination of fault planes from auxiliary planes based on simultaneous determination of stress tensor and a large number of fault plane solutions, *J. Geophys. Res.*, *100*, 8327–8338, 1995.

Jaeger, J. C., *Elasticity, Fracture and Flow*, 212 pp., Methuen & Co., London, 1964.

Jones, L. M., Focal Mechanisms and the State of Stress on the San Andreas Fault in Southern California, *J. Geophys. Res.*, *93*, 8869–8891, 1988.

Julien, Ph., and F. H. Cornet, Stress determination from focal mechanisms, *E.O.S. Trans. A.G.U.*, *67*(44), 1086, 1986.

Kerkela, S., and J. Stock, Compression directions north of the San Fernando Valley determined from borehole breakouts, *Geophys. Res. Lett.*, *23*(22), 3365–3368, 1996.

Lana, X., Estado de esfuerzos calculado a partir de un conjunto de mecanismos focales coherentes, *Rev. Geofisica, Madrid*, *42*, 53–62, 1986.

Lund, B., and R. Slunga, Stress tensor inversion using detailed microearthquake information and stability constraints: Application to Olfus in southwest Iceland, *J. Geophys. Res.*, *104*, 14,947–14,964, 1999.

McKenzie, D. P., The relation between fault plane solutions for earthquakes and the directions of the principal stresses, *Bull. Seismol. Soc. Am.*, *59*, 601–609, 1969.

Michael, A. J., Use of focal mechanisms to determine stress: A control study, *J. Geophys. Res.*, *92*, 357–368, 1987.

Michael, A. J., A genetic algorithm stress inversion method, *Seism. Res. Lett.*, *71*, 228, 2000.

Mueller, B., J. Reinecker, and K. Fuchs, The 2000 release of the World Stress Map, available online at http://www-wsm.physik.uni-karlsruhe.de/2000/, 2000.

Rivera, L., and A. Cisternas, Stress tensor and fault plane solutions for a population of earthquakes, *Bull. Seismol. Soc. Am.*, *80*, 600–614, 1990.

Vasseur, G. A., A. Etchecopar, and H. Philip, Stress state inferred from multiple focal mechanisms, *Ann. Geophys.*, *1*, 291–297, 1983.

Zhao, D., H. Kanamori, and D. Wiens, State of stress before and after the 1994 Northridge earthquake, *Geophys. Res. Lett.*, *24*, 519–522, 1997.

Zoback, M. D., and J. H. Healy, In situ stress measurements to 3.5 km depth in the Cajon Pass scientific research borehole: Implications for the mechanisms of crustal faulting, *J. Geophys. Res.*, *97*, 5039–5057, 1992.

Zoback, M. D., M. L. Zoback, V. S. Mount, J. Suppe, J. P. Eaton, J. H. Healy, D. H. Oppenheimer, P. A. Reasenberg, L. M. Jones, C. B. Raleigh, I. G. Wong, O. Scotti, and C. M. Wentworth, New evidence on the state of stress of the San Andreas Fault System, *Science*, *238*, 1105–1111, 1987.

———————————

H. Kanamori, Seismological Laboratory, California, Institute of Technology, Pasadena, CA 91125, USA.

L. Rivera, EOST-IPGS, Université Louis Pasteur, 5, Rue René Descartes, F67084, Strasbourg Cedex, France.